J. Am. Soc. Mass Spectrom. (2018) 29:1355–1364
DOI: 10.1007/s13361-018-1922-1

RESEARCH ARTICLE

Implementation of Precursor and Neutral Loss Scans on a Miniature Ion Trap Mass Spectrometer and Performance Comparison to a Benchtop Linear Ion Trap

Dalton T. Snyder, Lucas J. Szalwinski, Ryan Hilger, R. Graham Cooks

Department of Chemistry, Purdue University, West Lafayette, IN 47907, USA

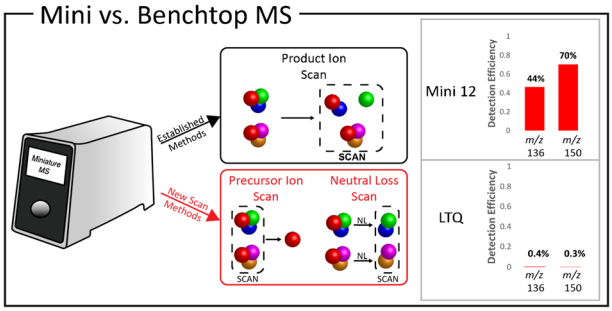

Abstract. Implementation of orthogonal double resonance precursor and neutral loss scans on the Mini 12 miniature rectilinear ion trap mass spectrometer is described, and performance is compared to that of a commercial Thermo linear trap quadropole (LTQ) linear ion trap. The ac frequency scan version of the technique at constant rf voltage is used here because it is operationally much simpler to implement. Remarkably, the Mini 12 shows up to two orders of magnitude higher sensitivity compared to that of the LTQ. Resolution on the LTQ is better than unit at scan speeds of ~ 400 Th/s, whereas peak widths on the Mini 12, on average, range from 0.5 to 2.0 Th full width at half maximum and depend heavily on the precursor ion Mathieu *q* parameter as well as the pump down time that precedes the mass scan. Both sensitivity and resolution are maximized under higher pressure conditions (short pump down time) on the Mini 12. The effective mass range of the product ion ejection waveform was found to be 5.8 Th on the Mini 12 in the precursor ion scan mode vs. that of 3.9 Th on the LTQ. In the neutral loss scan mode, the product ion selectivity was between 8 and 11 Th on the Mini 12 and between 7 and 8 Th on the LTQ. The effects of nonlinear resonance lines on the Mini 12 were also explored.

Keywords: Miniature mass spectrometer, MS/MS, Tandem mass spectrometry, Precursor ion scan, Neutral loss scan

Received: 3 November 2017/Revised: 8 January 2018/Accepted: 13 January 2018/Published Online: 13 March 2018

Introduction

Although product ion scans are common on single quadrupole ion traps, the two other main MS/MS scans (precursor scan and neutral loss scan) [1] are generally thought problematic on a single analyzer. Conventionally, these two survey scans are implemented on triple quadrupole mass spectrometers [2] wherein the first and third quadrupoles mass select particular precursor and product ions while an intermediate rf-only quadrupole serves as a collision cell. Such a scan is complicated on most single mass analyzers due to the difficulty in not only mass selecting multiple ions simultaneously, but also activating the precursor ion via collision-induced dissociation. A single quadrupole ion trap, however, can do both and hence can perform precursor and neutral loss scans via double resonance, that is, by simultaneously activating precursor ions and ejecting mass-selected product ions by applying multiple resonance (i.e., low-voltage auxiliary) frequencies [3–6].

Although single analyzer precursor and neutral loss scans do not compare favorably with data-dependent methods [7] on commercial mass spectrometer systems in terms of mass spectral resolution, sensitivity, and speed, they are more attractive on some miniature systems (see Introduction S1 in SI). Not only does the mass analyzer need to decrease in size on these smaller spectrometers [8–12], but so do the electronics and data acquisition systems, the ion optics (if there are any), and most importantly, the vacuum system. Because small vacuum pumps, usually a 10 L/s turbo pump backed by a 5 L/min

Electronic supplementary material The online version of this article (https://doi.org/10.1007/s13361-018-1922-1) contains supplementary material, which is available to authorized users.

Correspondence to: R. Cooks; *e-mail:* cooks@purdue.edu

diaphragm pump [13], struggle to pump a single chamber to < 1 Torr with a continuous atmospheric pressure interface, the discontinuous atmospheric pressure interface (DAPI) has become an attractive alternative [14, 15]. Continuous interfaces do exist on miniature spectrometers, but they are usually 2–3 orders of magnitude less sensitive than their discontinuous counterparts (e.g., Mini 10, 11, 12, S) [16–20]. Although efforts have been made to miniaturize ICRs [21], the Orbitrap [22], sector instruments [23, 24], and even a triple quadrupole mass spectrometer [25], for the reasons above—especially vacuum system constraints—the quadrupole ion trap has become the predominant analyzer for miniaturization. Conventionally, this would limit miniature mass spectrometers to the full scan mode and the product ion scan mode, and in combination with the long pump down time characteristic of DAPI systems (10^{-1}–10^{0} s), reconstructing precursor and neutral loss spectra from data-dependent sets of product ion scans becomes less feasible. However, if operated unconventionally in the ac frequency scan mode [26–28], precursor and neutral loss scan modes become available, somewhat mitigating the need for another analyzer for higher resolution or improved MS/MS capabilities and providing an attractive alternative over conventional data-dependent modes.

In this study, we implemented capabilities for precursor ion scanning and neutral loss scanning on a Mini 12 miniature rectilinear ion trap mass spectrometer and compared their performance to that obtained on a commercial Thermo linear trap quadropole (LTQ) linear ion trap. Both resolution and limit of detection were characterized as well as detection efficiency and mass-to-charge selectivity. Nonlinear resonance lines were also explored.

Experimental

Chemicals

Amphetamine (*m/z* 136), methamphetamine (*m/z* 150), 3,4-methylenedioxyamphetamine (*m/z* 180), 3,4-methylenedioxymethamphetamine (*m/z* 194), and 3,4-methylenedioxyethylamphetamine (*m/z* 208) were purchased from Cerilliant (Round Rock, TX, USA). HPLC grade methanol was purchased from Fisher Scientific (Hampton, NH, USA). Formic acid was purchased from Sigma-Aldrich (St. Louis, MO, USA). All analytes were diluted in methanol with 0.1% formic acid. A concentration of 1 ppm was used for all experiments except when a calibration curve was made.

Ionization

Nanoelectrospray ionization using a 1.5-kV potential was utilized for all experiments. Borosilicate glass capillaries (1.5-mm O.D., 0.86-mm I.D.) from Sutter Instrument Co. (Novato, CA, USA) were pulled to 2-μm tip diameters using a Flaming/Brown micropipette puller (model P-97, Sutter Instrument Co.). The nanospray electrode holder (glass size 1.5 mm) was purchased from Warner Instruments (Hamden, CT, USA) and was fitted with 0.127-mm-diameter silver wire, part number 00303 (Alfa Aesar, Ward Hill, MA), as the electrode.

Instrumentation

Experiments were performed on the homebuilt Mini 12 miniature ion trap mass spectrometer. The Mini 12 has a rectilinear ion trap (RIT, $x_0 = 5.0$ mm, $y_0 = 4.0$ mm, length 43.2 mm) with slits of length 15.0 mm and width 1.0 mm on the x electrodes [19, 20, 29]. The main trapping radiofrequency (rf) voltage (~ 5 kV_{pp} max, 1.017 MHz) is generated by an LC tank circuit (Fig. 1, black) and is normally applied only to the y rods while the x rods are either grounded or used for applying low-voltage ac signals. Endcap lenses operated at ~ 50 V keep ions trapped axially. A single conversion dynode with electron multiplier (model 397, DeTech Detector Technology, Inc., MA) is used for detection. The ion trap typically operates in the resonance ejection mode [30] and has custom-designed electronics for linearly ramping the rf voltage, applying low-voltage ac frequencies to the x rods for stored waveform inverse Fourier transform isolation (or activation) [31–33] and collision-induced dissociation (MS^n), and low- and high-voltage DC signals for the endcap electrodes and conversion dynode/electron multiplier, respectively. High voltage (up to 5 kV) can also be supplied by the Mini 12 for ionization.

The Mini 12 uses a discontinuous atmospheric pressure interface [14]. Ions and neutrals are admitted into the Mini 12 RIT by opening the DAPI valve for ~ 12 ms, after which the valve is closed and a wait time is used for collisional cooling. During this time, the pressure in the ion trap drops from 10^{-1} Torr to between 10^{-3} and 10^{-5} Torr, during which mass analysis or collision-induced dissociation takes place.

The performance of the Mini 12 was compared to that of a commercial LTQ linear ion trap mass spectrometer (Thermo Finnigan, San Jose, CA, USA). The LTQ has a three-section linear ion trap with hyperbolic cross sections. The dimensions of the device are $x_0 = 4.75$ mm, $y_0 = 4$ mm, and three axial sections of lengths 12, 37, and 12 mm. The rf was tuned to 1.166 MHz. The LTQ uses helium (ion gauge reading 0.60×10^{-5} Torr) as the cooling and collision gas, whereas the Mini 12 uses air with a base pressure of 10^{-5} Torr. Importantly, the Mini 12 uses a single-electron multiplier with conversion dynode as the detector, whereas the LTQ uses two, one on either side of the linear ion trap.

The Mini 12 rf circuit was modified as shown in Fig. 1, in red. A center-tapped iron core toroidal transformer (Laird Technologies LFB090050-000, Earth City, MO, USA) enabled coupling of low-voltage ac signals on the y electrodes. The coils on the toroid do not overlap in order to improve isolation between the rf and ac signals. The ac signal is applied to the primary winding, and the two outputs of the secondary winding are applied to the two y rods, giving a dipolar ac signal between the rods. The rf signal is a single phase on the y rods, and low-voltage ac signals are applied directly to the x rods. The LTQ rf coil was modified as described previously [5, 6] with an extra Thermo LTQ low pass filter board (part 97055−91120) and

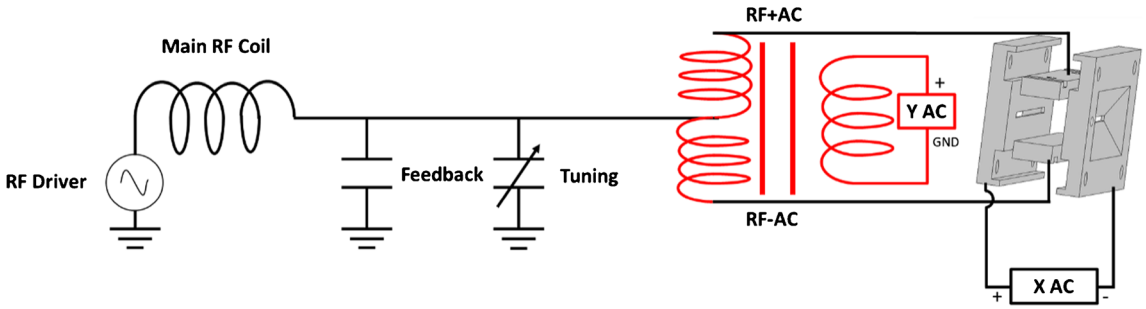

Figure 1. Schematic of existing Mini 12 rf coil coupled to the rectilinear ion trap (black) and center-tapped toroidal transformer (red) used to couple low-voltage ac signals onto the y rods

Thermo LTQ balun board (part 97055−91130) in order for low-voltage ac signals to be applied to both x and y electrodes of the linear ion trap.

Two Keysight 33612A arbitrary waveform generators (Newark element14, Chicago, IL, USA) were used to apply low-voltage ac waveforms to the x and y electrodes of each linear ion trap. One generator supplied the waveform for the x electrodes and one supplied the waveform for the y electrodes. The sampling rate of arbitrary waveforms was set at 10 megasamples per second.

Waveforms

Precursor ion scans require application of (1) an ac frequency sweep (at constant rf voltage) for mass-selective precursor ion excitation and (2) a fixed frequency of higher amplitude for ejection of a particular product ion [3, 5, 34]. Neutral loss scans require three simultaneous and identical frequency sweeps with appropriate trigger delays: a first sweep for precursor ion excitation, a second sweep for ejection of leftover precursor ions into the y electrodes, and a third frequency sweep for ejection of the neutral loss product ions in the x dimension. The trigger delay between precursor excitation and product ion ejection is directly proportional to the neutral loss. Generally, excitation amplitude was 200–300 mV_{pp} and ejection amplitude was 600–800 mV_{pp}. Excitation and artifact rejection signals were applied to the y rods and ejection signals were applied to the x rods, usually each in a dipolar fashion. All frequency sweeps in this work are inverse Mathieu q scans [35] that linearize the mass scale with respect to time by sweeping the ac frequency nonlinearly. These waveforms generally started at Mathieu $q = 0.908$ and ended at $q = 0.3$ with a sweep time of 600 ms. They were calculated in Matlab according to previously described methods [35] and imported to the Keysight waveform generators.

Scan Functions

The Mini 12 scan function is as follows: ion injection (DAPI open), 12 ms; cooling (DAPI closed, instrument pump down), 700 ms; ramp rf voltage up to operating point, 100 ms; mass scan, 600 ms; reset for next scan, 1 ms. The function generators were triggered by a 5-V pulse that normally operates the "Sample Pump" as a 24-V pulse. A voltage divider was used to obtain the former from the latter. Data were acquired at 312,500 samples per second and were digitally smoothed using a 30-point triangle filter.

The LTQ was operated in the "Ultrazoom" mode with an ion injection time of 10 ms. The rf voltage was constant throughout the ion injection, cooling, and mass scan and was controlled externally by substituting the coil modulation signal (proportional to the rf amplitude) on the rf detector board with a dc signal from an external function generator. Automatic gain control was turned off throughout this study, but space charge was not observed at 1-ppm concentration as demonstrated in SI Figure S1. The three function generators were triggered by the "Injection" trigger in the LTQ Tune "Diagnostics" menu. The data collection rate on the LTQ was approximately 2700 samples per second.

In all experiments, m/z 119 had its working point at a Mathieu q value of 0.57 on LTQ vs. 0.53 on the Mini 12.

Data Interpretation

Data were analyzed in either Matlab (Mathworks, Natick, MA, USA) or Excel (Microsoft, Redmond, WA, USA). Spectra were mass calibrated separately using a linear fit of m/z vs. time. In most cases, Mini 12 spectra are the average of three separate scans, whereas the LTQ data is the average of 10 scans. In the case of the LTQ, the only scan saved was the average spectrum and hence error bars will not be shown for LTQ data. All ion intensities are baseline-subtracted integrated intensities. Resolution is dimensionless and is reported as $m/\Delta m$, where m is the m/z value of the precursor ion (Th) and Δm is the measured full (peak) width at half maximum intensity (FWHM), also in Th.

Results and Discussion

Five amphetamine standards were chosen for this study, using transitions given as follows: amphetamine (m/z 136–> m/z 119), methamphetamine (m/z 150–> m/z 119), 3,4-methylenedioxyamphetamine (m/z 180–> m/z 163), 3,4-methylenedioxymethamphetamine (m/z 194–> m/z 163), and 3,4-methylenedioxyethylamphetamine (m/z 208–> m/z 163). Of interest here is not any particular class of compounds or implementation with a particular ion source, but rather performance metrics. Characterized here are mass spectral resolution,

sensitivity, detection efficiency, product ion selectivity, pressure effects, and nonlinear resonance lines. We further compare the performance of the Mini 12 to that of a benchtop LTQ linear ion trap in both the precursor ion and neutral loss scan mode, an overview of which is shown in Table 1.

Performance of Precursor and Neutral Loss Scans

A full scan mass spectrum of the five-component amphetamine mixture obtained on the Mini 12 is shown in Fig. 2a. Fragmentation is observed even in the full scan, with *m/z* 163, *m/z* 119, and *m/z* 91 all present. This fragmentation can be attributed to the large pressure change during ion injection, during which the precursor ions can fragment. The lower limit of the mass spectra here is set at *m/z* 120 since the lowest *m/z* fragment interrogated is *m/z* 119, and hence any precursor or neutral loss scan peaks below this are artefactual for singly charged ions.

Both precursor ion scans of *m/z* 119 (for amphetamine and methamphetamine) and *m/z* 163 (for the other three) are shown in Fig. 2b, c. A double simultaneous precursor ion scan is then shown in Fig. 2d. This spectrum was obtained by applying the resonance frequency of *m/z* 119 on one of the x rods and simultaneously applying the resonance frequency of *m/z* 163 on the other x rod while sweeping the excitation frequency on the y rods. The corresponding neutral loss scans of 17 and 31 Da are shown in panels e and f. Note that *m/z* 163 (a fragment of *m/z* 180, 194, and 208) is detected because it fragments to *m/z* 133 and 135 and the neutral loss scan does not have unit selectivity. Corresponding precursor and neutral loss scans on the LTQ are shown in Figure S2 (helium bath gas) and Figure S3 (nitrogen bath gas). The use of nitrogen as bath gas increases the integrated signal intensity but also compromises resolution.

Sensitivity and Limit of Detection

Sensitivity and limit of detection are two performance metrics that were characterized on both the Mini 12 and LTQ. The precursor ion scan of *m/z* 119 was used for this experiment. The concentrations of amphetamine and methamphetamine were varied over four orders of magnitude from 10 ppb (viz. ng/mL) to 100 ppm (viz. μg/mL). The integrated signal intensity was plotted against concentration to obtain a semi-quantitative calibration curve. Because internal standards were not used, the linearity of the plots is less than ideal. Therefore, we defined the limit of detection as the concentration of reagents which yielded the mass spectrum with signal-to-noise ratio of 3. On the Mini 12 (Fig. 3a), the limit of detection for the precursor ion scan was 10 ppb, whereas the detection limit using the same frequency scan rate for excitation on the LTQ was 1 ppm (Fig. 3c). Note that the LTQ uses two detectors whereas the Mini 12 uses one. For comparison, the LTQ's product ion scan mode ($q_{exc} = 0.25$, 30 ms excitation time, normalized collision energy of 25) yielded a limit of detection of 1 ppb for both *m/z* 136 and *m/z* 150 (Figure S4).

The remarkable difference between limits of detection on the Mini 12 and LTQ in the precursor ion scan mode can likely be explained by several factors. First, the Mini 12 uses air as collision gas whereas the LTQ uses helium, which affects fragmentation efficiency and collisional damping (the latter being important to cool the product ions to the center of the trap before they are ejected in the x dimension). The higher operating pressure on the Mini 12 helps with these processes. Substituting nitrogen for helium in the LTQ gave a limit of detection of 250 ppb on the LTQ in the precursor ion scan mode (Figure S5a), and the sensitivity (slope of the calibration curve) increased by a factor of 2.6 for *m/z* 136 and 5.8 for *m/z* 150.

A calibration curve was also constructed for the neutral loss scan of 31 Da. Solutions used for this experiment consisted solely of methamphetamine and 3,4-methylenedioxymethamphetamine at various concentrations. The calibration curve on the Mini 12 for both *m/z* 150 and 194 is shown in Fig. 3b. Surprisingly, even at 1 ppm concentration, there is loss of calibration linearity. The limit of detection (S/N = 3) was found to be 250 ppb, much higher than that of the precursor ion scan and reasonably comparable to the LTQ's 500-ppb detection limit in the neutral loss scan mode using helium as bath gas (Fig. 3d). Using nitrogen as bath gas on the LTQ resulted in a limit of detection of 250 ppb (Figure S5b) due to a doubling in sensitivity.

Both the severe increase in limit of detection and loss of calibration curve linearity on the Mini 12, even at high concentrations (1 ppm), are somewhat puzzling. Space charge may play a role here but is unlikely to be the only factor since it was not observed at 1 ppm in the full scan mode or in the other MS/MS scan modes on the Mini 12 and LTQ. However, there are key differences between the precursor scan and neutral loss scan that are worth considering. We postulate that the loss in calibration linearity is due to frequency shifts in the Mini 12 ion trap [36, 37]. As the precursor ions are excited, they approach the y electrodes where their secular frequencies shift. Because the product ions are then generated close to the y electrodes, their secular frequencies are shifted relative to their "true" or predicted secular frequencies. Their y oscillations then dampen rapidly in the ion trap due to collisions with air molecules, returning their secular frequencies to the "normal" predicted values. At the same time, their x amplitudes increase via the ejection frequency sweep, again shifting their frequencies. It is this combination of frequency shifts, exacerbated by the fact that the precursor and product ion ejection waveforms must be swept at a *constant mass offset* that may cause loss of calibration linearity and also an increase in limit of detection.

Detection Efficiency

We next measured the percentage of precursor ions that were converted to product ions that were detected, which we define as the "detection efficiency." The detection efficiency is thus affected by fragmentation efficiency of the precursor ions, product ion collisional cooling, and product ion ejection efficiency. Detection efficiency was calculated as the ratio,

Table 1. Performance of Precursor and Neutral Loss Scans on LTQ (helium bath gas) and Mini 12 (air)

Performance metric	LTQ Pre	Mini 12 Pre	LTQ NL	Mini 12 NL
Resolution ($m/\Delta m$) at m/z 150	300	150	300	150
Product ion selection window (m/z 136, m/z 150)	3.9, 4.3 Th	5.6, 5.6 Th	7.1, 7.8 Th	8.6, 11 Th
Limit of detection (ppb)[a]	1000	10	500	250
Detection efficiency[a]	0.3–0.4%	40–80%	1–3%	40–70%

In these experiments, the rf voltage was set such that m/z 119 was placed at $q = 0.53$ (Mini 12) or $q = 0.57$ (LTQ)
Pre precursor ion scan of m/z 119, *NL* neutral loss scan of 31 Da
[a]LTQ has two detectors and Mini 12 has a single detector

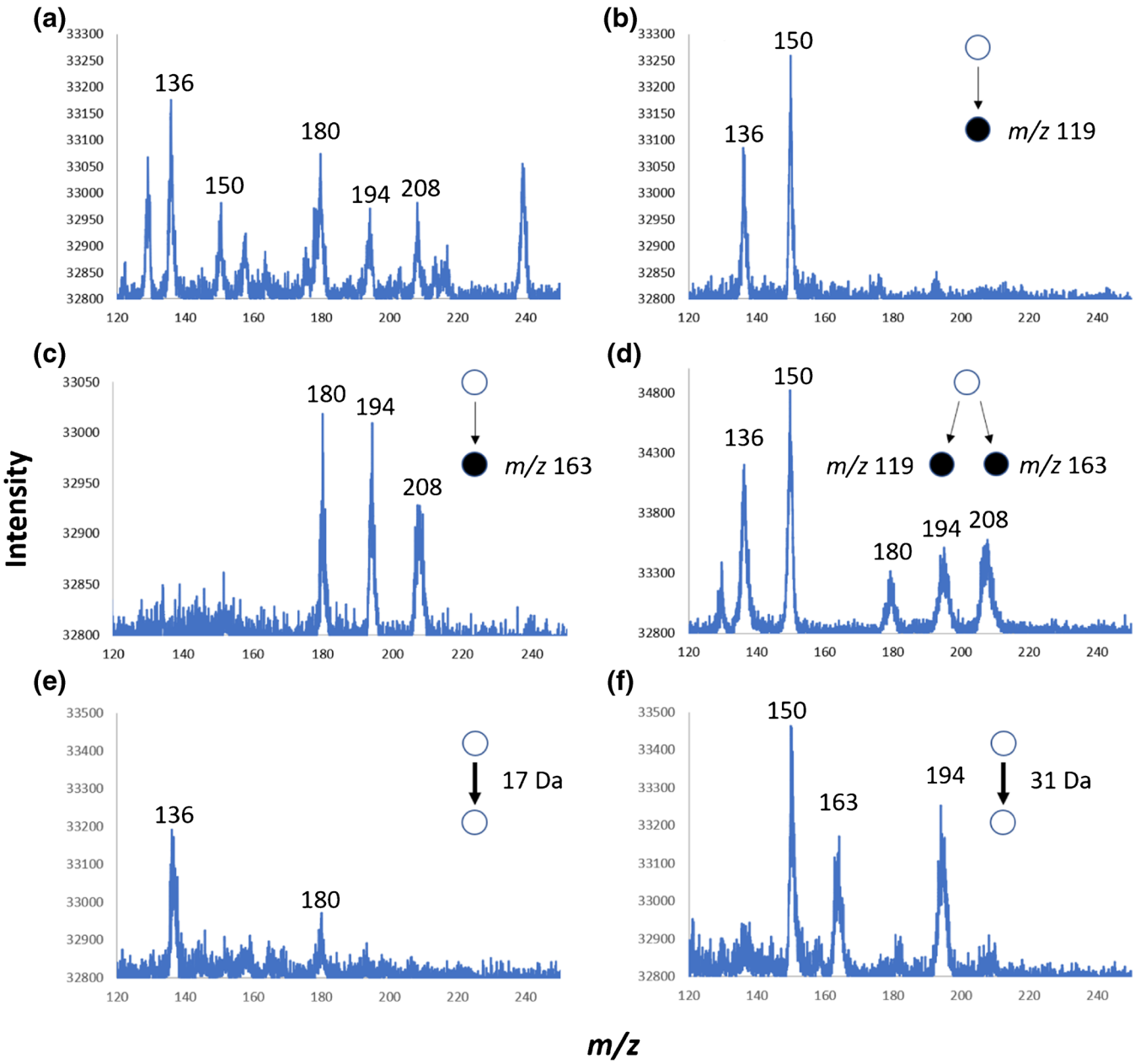

Figure 2. Precursor and neutral loss scans on the Mini 12 mass spectrometer: **a** Full ac frequency scan mass spectrum of five amphetamines (m/z 136, 150, 180, 194, and 208). **b** Precursor ion scan of m/z 119. **c** Precursor ion scan of m/z 163. **d** Double simultaneous precursor scan of m/z 119 and m/z 163. **e** Neutral loss scan of 17 Da. **f** Neutral loss scan of 31 Da. These data can be compared to corresponding LTQ spectra in the Supplemental Information (Figures S1, S2, S3)

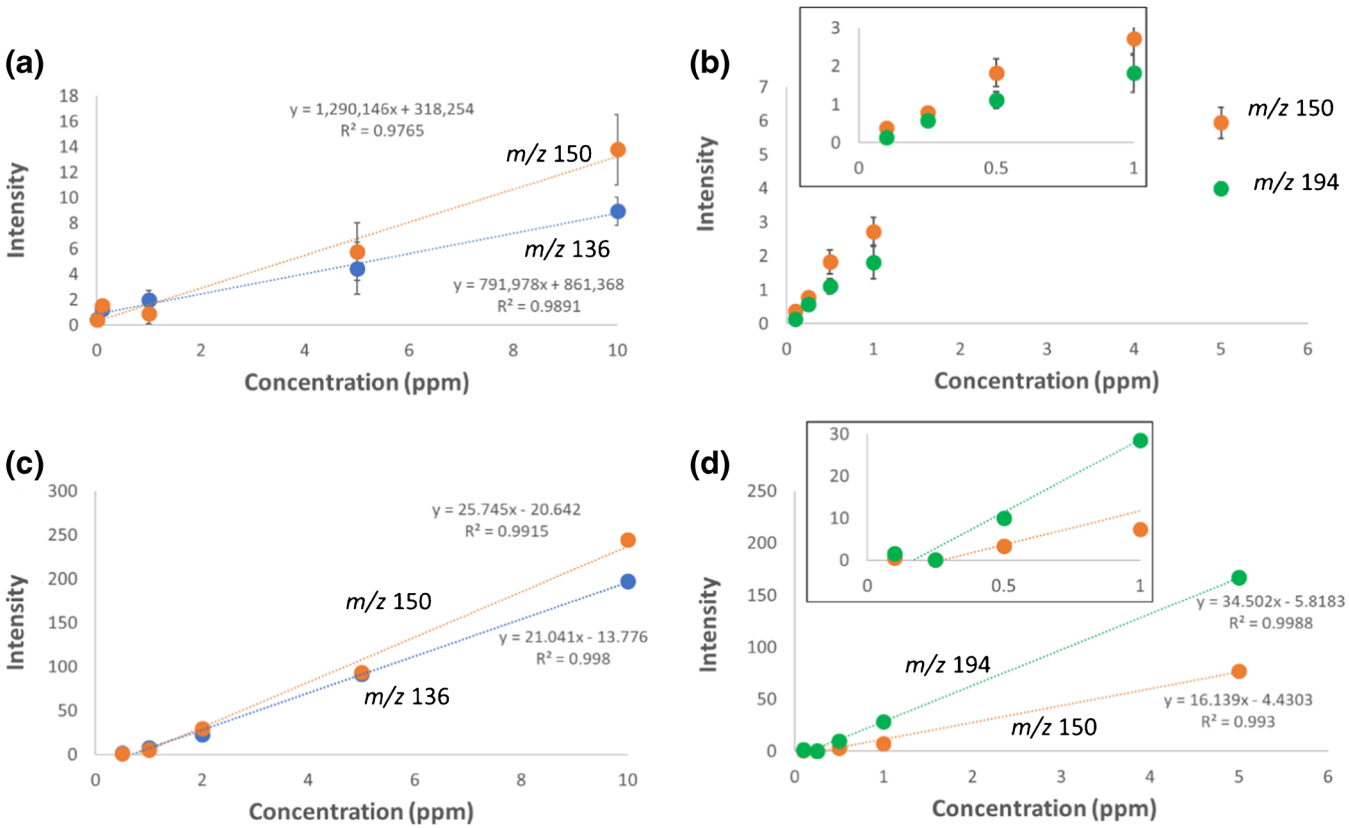

Figure 3. Panel (**a**) is the precursor ion scan of *m/z* 119 on the Mini 12, panel (**b**) is the neutral loss scan of 31 Da on the Mini 12, panel (**c**) is the precursor ion scan of *m/z* 119 on the LTQ, and panel (**d**) is the neutral loss scan of 31 Da on the LTQ. LTQ calibration curves using nitrogen are shown in Figure S5

expressed as a percent, of integrated peak intensity for ions of a selected *m/z* in the precursor or neutral loss scan to the integrated peak intensity measured using mass-selective instability with resonance ejection (see Discussion S1 in SI). As shown in Fig. 4a, the detection efficiency on the Mini 12 was two orders of magnitude higher, 44% for amphetamine and 70% for methamphetamine vs. 0.4 and 0.3%, respectively, than that for the LTQ (helium bath gas) in the precursor scan of *m/z* 119. If we consider, though, that the LTQ has two detectors to the Mini 12's one, then, the corresponding detection efficiencies on the LTQ were 0.2 and 0.15%, respectively. Substituting nitrogen for helium in the LTQ resulted in 2.6 and 4.8% efficiencies. For the neutral loss scan of 31 Da, the Mini 12 yielded 38 and 67% efficiencies for *m/z* 150 and 194, respectively, to those of the LTQ 1.1 and 2.6% using helium gas (Fig. 4b). Nitrogen improved LTQ efficiencies to 10.4 and 8.0%.

Resolution and Product Ion Selectivity

Resolution in ac frequency scanning depends heavily upon the frequency dispersion of the trapped ions as well as their secular frequency bandwidths [38]. It is thus important to characterize both *mass spectral resolution* and the *product ion selection window*.

At an rf amplitude of 7000 DAC units (LMCO ~ 70 Th), peak widths on the Mini 12 were 1.48 and 1.86 Th for *m/z* 136 and 150, respectively, whereas for an rf amplitude of 9500 DAC units (LMCO ~ 92 Th), peak widths decreased to 0.93 and 0.87 Th. Unfortunately, at higher rf amplitudes, artifact peaks were observed because the amphetamine precursor ions fragment to *m/z* 91 as well, and so if the precursors fragment while the LMCO > 91 Th, the product ion *m/z* 91 will inadvertently be detected by boundary instability. In the case of the LTQ, unit resolution was observed for a LMCO of 87 Th, with approximate peak widths of 0.5 Th for *m/z* 136 and 150. In nitrogen, the peak width for *m/z* 136 was 1.1 Th and for *m/z* 150 was 0.9 Th. On both the Mini 12 and LTQ, resolution degraded at lower Mathieu *q* values due to decreased secular frequency dispersion.

We define the product ion selection window for the precursor ion scan as $\Delta(m/z)$, or the width (in Th) of the intensity vs. product ion ejection frequency curve as measured at half maximum amplitude. In other words, the product ion selection window describes the range of *m/z* values that are targeted by the ejection frequency in the MS/MS scan: $(m/z)_{\text{precursor}} -> (m/z)_{\text{product}} \pm \Delta(m/z)/2$. In this experiment, a precursor ion scan of *m/z* 119 was performed on amphetamine and methamphetamine and the ejection frequency was altered from its ideal value of 201 kHz (Mini 12, $q = 0.53$) and 253 kHz (LTQ, $q = 0.57$). The integrated intensities of *m/z* 136 and 150 were recorded. On the Mini 12, the FWHM of the curve was 5.6 Th (Fig. 5a), compared to that of

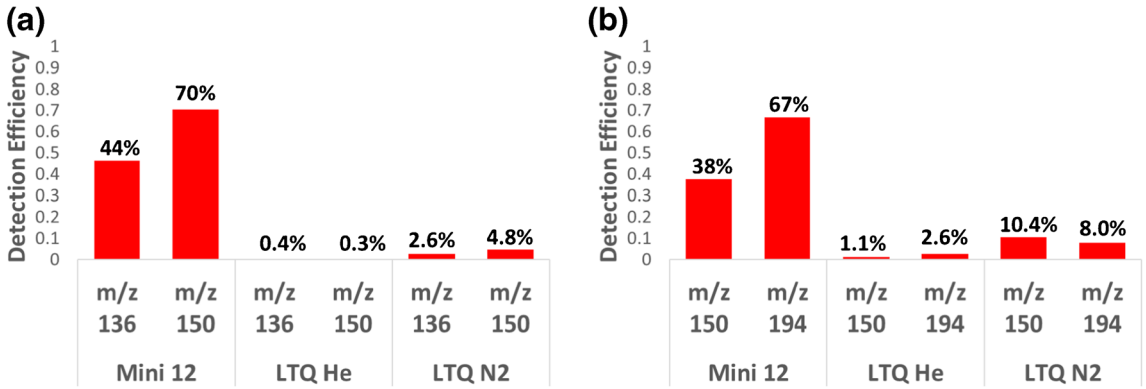

Figure 4. Detection efficiencies for precursor ion scan of *m/z* 119 (**a**) and neutral loss scan of 31 Da (**b**) on the Mini 12 and LTQ (helium or nitrogen bath gas). The detection efficiency was calculated as the ratio of MS/MS scan intensity to full MS scan intensity (and expressed as a percent) for the selected ion

approximately 3.9 Th (*m/z* 136) and 4.3 Th (*m/z* 150) on the LTQ using helium (Fig. 5b). In other words, on the Mini 12, ions between *m/z* 121.5 and *m/z* 115.9 were selected for ejection from the trap by applying an 800-mV_{pp} excitation signal corresponding to the secular frequency of *m/z* 119.

In order to determine the product ion selection window (in Th) for the neutral loss scan of 31 Da, the trigger delay between the precursor excitation frequency sweep and both the artifact rejection sweep and product ejection sweep was varied while keeping the difference between the artifact rejection trigger delay and product ejection trigger delay constant. The same rf amplitude, frequency scan rate, and ac voltages were used in this experiment as compared to those of the precursor scan experiment. The integrated intensities of methamphetamine and 3,4-methylenedioxymethamphetamine were plotted with respect to the trigger delays, and the results are shown in Fig. 5c (Mini 12) and d (LTQ, helium). For the Mini 12, the approximate product ion selection windows were 8.6 and 11 Th for *m/z* 150 and 194, respectively. For the LTQ, those widths were 7.1 and 7.8 Th, respectively. Other factors, such as mass scanning rate, that affect resolution are mentioned in Discussion S2.

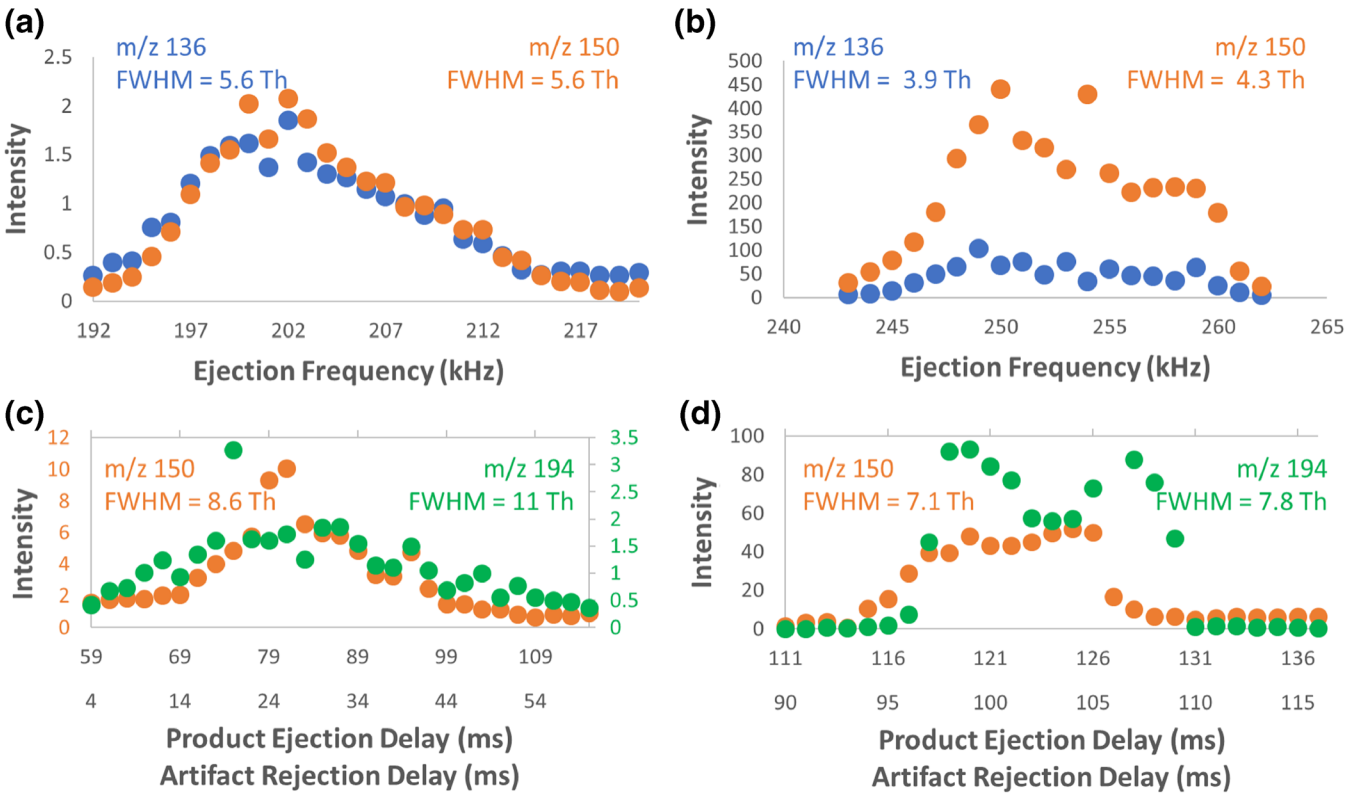

Figure 5. Product ion selection window in the precursor ion scan of *m/z* 119 on Mini 12 (**a**) and LTQ (**b**) and product ion selection window for the neutral loss scan of 31 Da on Mini 12 (**c**) and LTQ (**d**). FWHM, full width at half maximum of the ion intensity vs. ejection frequency (for the precursor scan) or trigger delay (for the neutral loss scan), which describes the range of product ion *m/z* values that are targeted by the given scan

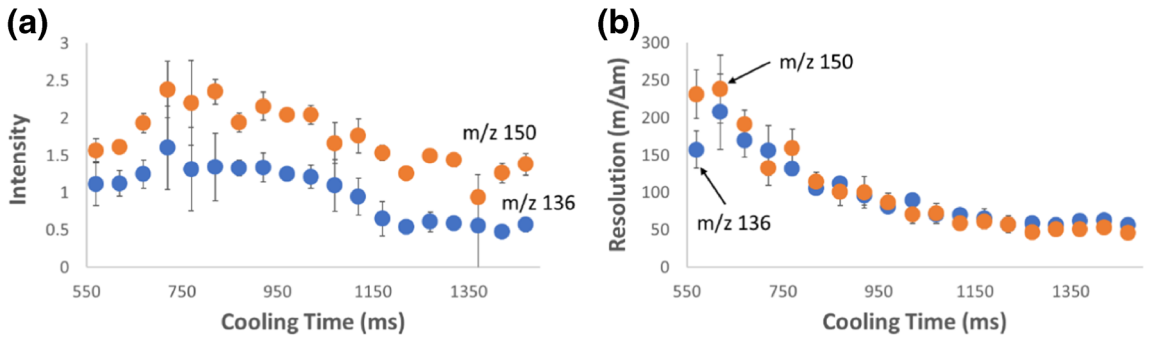

Figure 6. Effect of cooling time on precursor ion scan of *m/z* 119. **a** Ion intensity vs. cooling time. **b** Mass spectral resolution vs. cooling time. Data acquired on the Mini 12

Effect of Cooling Time

Although not a significant concern on a benchtop instrument which operates at constant pressure in the ion trap volume, pump down time on the Mini 12 must be carefully considered. The Mini 12 uses a discontinuous atmospheric pressure interface [14] composed of a silicone tube that is constricted by a pinch valve except for when ions are introduced. During ion introduction, a low-voltage pulse opens the valve, thereby letting ions and neutrals into the vacuum chamber. The ions are then trapped and cooled, and the chamber is pumped down to operating pressure. Because the pressure in the Mini 12 varies as a function of time, it is critical to optimize it for the given scan mode.

The effect of cooling time (i.e., instrument pump down time) on the sensitivity and resolution of the precursor ion scan of *m/z* 119 is shown in Fig. 6a, b, respectively. At low cooling times (high pressure), the peak width is minimized (panel b) at 0.94 and 0.56 Th for *m/z* 136 and 150, respectively, resulting in the best resolution. At high cooling times, the peak widths increase substantially to 2.5 and 3.3 Th, respectively, and the ion intensity also decreases, likely due to inefficient fragmentation at low pressure. In the middle (~ 750 ms), however, there is optimal ion intensity and reasonable peak width (1.0- and 1.1-Th peak widths for *m/z* 136 and 150).

Nonlinear Resonance Lines

Nonlinear resonance lines cause the rapid uptake of energy from the rf field so that any ion whose working point lies on the resonance line can be rapidly ejected even before a mass scan takes place [39–44]. Their effects on the spectra described here are thus important to consider, especially since the Mini 12 uses a single-section rectilinear ion trap which is only 65% quadrupolar with $A_4/A_2 = 7.9\%$ and $A_6/A_2 = -17.2\%$ [29]. In contrast, the LTQ houses a three-section trap (to minimize ion excursion into fringe fields near the endcaps) with hyperbolic cross sections [30]. Using the precursor ion scan of *m/z* 119 on the Mini 12 (while varying the rf voltage to change the ion's working point), we found that when *m/z* 136 had its working point placed at a black hole octupole line at $\beta = 1/2$ during the scan, the peak disappeared (Fig. 7, left). Moving the precursor ion working point away from the "black hole" increased the intensity of *m/z* 136 until it was far enough away that the nonlinear resonance appeared to have no effect (Fig. 7, right). These

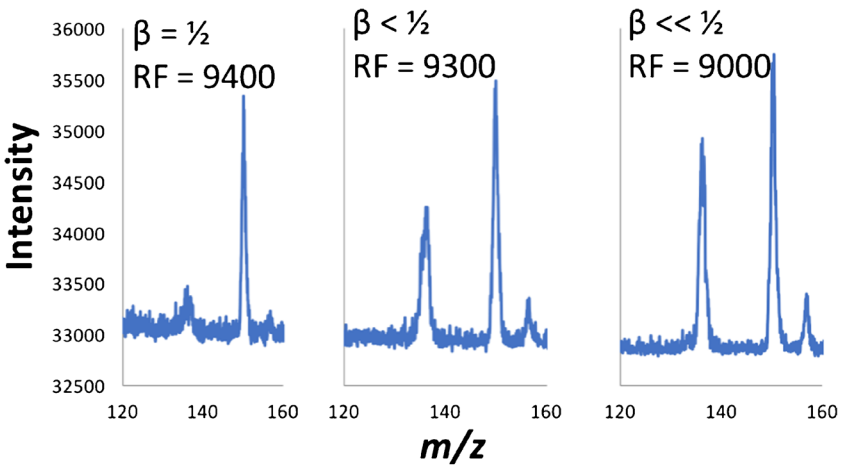

Figure 7. Effect of the octupole ($\beta = 1/2$) nonlinear resonance line on precursor ion scan of *m/z* 119. Precursor ion *m/z* 136 had working point either (left) on the nonlinear resonance line, (middle) slightly below the nonlinear resonance line, or (right) far away from the nonlinear resonance line. The working point of the ions was altered by changing the rf voltage (reported in DAC units) during the precursor ion scan

are identical results to our prior secular frequency scanning study [38]. When the *product ion* (*m/z* 119) was placed on or near the octupole nonlinear resonance line, no effect was observed. This is perhaps because the product ion is intended to be immediately ejected by the product ion ejection frequency so that any additional energy uptake due to the nonlinear resonance only helps in this process. However, the resolution did not increase compared to when the product ion was placed away from the nonlinear resonance line (experiment described in Discussion S3). We believe this is because the resolution is largely determined by the slow fragmentation of the precursor ions rather than the comparatively fast ejection of the product ions.

Conclusion

Precursor and neutral loss scans using orthogonal double resonance excitation have been successfully implemented on a miniature rectilinear ion trap. Compared to a selected benchtop instrument, the Mini 12 offers up to two orders of magnitude higher sensitivity in the precursor scan mode and 2× better sensitivity in the neutral loss scan mode. Future work should focus on improving the product ion selection window, which limits the selectivity of both types of MS/MS scans, as well as reducing the contribution of artifact peaks (from boundary instability).

The scans demonstrated here are particularly valuable for miniature instruments that use discontinuous interfaces, as they have very low duty cycles and will also be expected to have higher sensitivity by using a heavier collision gas. A goal of this work is to implement these scan modes at NASA Goddard Space Flight Center for possible use in future planetary missions [45, 46]. This would build on the importance of mass spectrometry in many NASA and European Space Agency missions including the Rosetta project [47, 48] and the more recent development of the Sample Analysis at Mars suite and Mars Organic Molecule Analyzer [49, 50].

Acknowledgements

Rob Schrader (Purdue University) is thanked for the Table of Contents graphic.

Funding Information

The authors acknowledge funding from NASA Planetary Sciences Division, Science Mission Directorate (NNX16AJ25G). This work was also supported by a NASA Space Technology Research Fellowship (DTS).

References

1. Schwartz, J.C., Wade, A.P., Enke, C.G., Cooks, R.G.: Systematic delineation of scan modes in multidimensional mass spectrometry. Anal. Chem. ***62***, 1809–1818 (1990)
2. Yost, R.A., Enke, C.G.: Triple quadrupole mass spectrometry for direct mixture analysis and structure elucidation. Anal. Chem. ***51***, 1251–1264 (1979)
3. Johnson, J.V., Pedder, R.E., Yost, R.A.: MS-MS parent scans on a quadrupole ion trap mass-spectrometer by simultaneous resonant excitation of multiple ions. Int. J. Mass Spectrom. Ion Process. ***106***, 197–212 (1991)
4. Snyder, D.T., Szalwinski, L., Cooks, R.G.: Simultaneous and sequential MS/MS combinations and permutations in a linear quadrupole ion trap. Anal. Chem. ***89***, 11053–11060 (2017)
5. Snyder, D.T., Cooks, R.G.: Single analyzer precursor ion scans in a linear quadrupole ion trap using orthogonal double resonance excitation. J. Am. Soc. Mass Spectrom. ***28***, 1929–1938 (2017)
6. Snyder, D.T., Cooks, R.G.: Single analyzer neutral loss scans in a linear quadrupole ion trap using orthogonal double resonance excitation. Anal. Chem. ***89***, 8148–8155 (2017)
7. McClellan, J.E., Quarmby, S.T., Yost, R.A.: Parent and neutral loss monitoring on a quadrupole ion trap mass spectrometer: screening of acylcarnitines in complex mixtures. Anal. Chem. ***74***, 5799–5806 (2002)
8. Badman, E.R., Cooks, R.G.: Miniature mass analyzers. J. Mass Spectrom. ***35***, 659–671 (2000)
9. Blain, M.G., Riter, L.S., Cruz, D., Austin, D.E., Wu, G., Plass, W.R., Cooks, R.G.: Towards the hand-held mass spectrometer: design considerations, simulation, and fabrication of micrometer-scaled cylindrical ion traps. Int. J. Mass Spectrom. ***236***, 91–104 (2004)
10. Tian, Y., Higgs, J., Li, A., Barney, B., Austin, D.E.: How far can ion trap miniaturization go? Parameter scaling and space-charge limits for very small cylindrical ion traps. J. Mass Spectrom. ***49***, 233–240 (2014)
11. Wu, Q., Li, A., Tian, Y., Zare, R.N., Austin, D.E.: Miniaturized linear wire ion trap mass analyzer. Anal. Chem. ***88***, 7800–7806 (2016)
12. Tian, Y., Decker, T.K., McClellan, J.S., Bennett, L., Li, A., De la Cruz, A., Andrews, D., Lammert, S.A., Hawkins, A.R., Austin, D.E.: Improved Miniaturized Linear Ion Trap Mass Spectrometer Using Lithographically Patterned Plates and Tapered Ejection Slit. J. Am. Soc. Mass Spectrom. ***29***, 213–222 (2018)
13. Chen, C.H., Chen, T.C., Zhou, X., Kline-Schoder, R., Sorensen, P., Cooks, R.G., Ouyang, Z.: Design of portable mass spectrometers with handheld probes: aspects of the sampling and miniature pumping systems. J. Am. Soc. Mass Spectrom. ***26***, 240–247 (2015)
14. Gao, L., Cooks, R.G., Ouyang, Z.: Breaking the pumping speed barrier in mass spectrometry: discontinuous atmospheric pressure interface. Anal. Chem. ***80***, 4026–4032 (2008)
15. Wei, Y., Bian, C., Ouyang, Z., Xu, W.: A pulsed pinhole atmospheric pressure interface for simplified mass spectrometry instrumentation with enhanced sensitivity. Rapid Commun. Mass Spectrom. ***29***, 701–706 (2015)
16. Riter, L.S., Peng, Y., Noll, R.J., Patterson, G.E., Aggerholm, T., Cooks, R.G.: Analytical performance of a miniature cylindrical ion trap mass spectrometer. Anal. Chem. ***74***, 6154–6162 (2002)
17. Gao, L., Song, Q., Patterson, G.E., Cooks, R.G., Ouyang, Z.: Handheld rectilinear ion trap mass spectrometer. Anal. Chem. ***78***, 5994–6002 (2006)
18. Gao, L., Sugiarto, A., Harper, J.D., Cooks, R.G., Ouyang, Z.: Design and characterization of a multisource hand-held tandem mass spectrometer. Anal. Chem. ***80***, 7198–7205 (2008)
19. Hendricks, P.I., Dalgleish, J.K., Shelley, J.T., Kirleis, M.A., McNicholas, M.T., Li, L., Chen, T.C., Chen, C.H., Duncan, J.S., Boudreau, F., Noll, R.J., Denton, J.P., Roach, T.A., Ouyang, Z., Cooks, R.G.: Autonomous in situ analysis and real-time chemical detection using a backpack miniature mass spectrometer: concept, instrumentation development, and performance. Anal. Chem. ***86***, 2900–2908 (2014)
20. Li, L., Chen, T.C., Ren, Y., Hendricks, P.I., Cooks, R.G., Ouyang, Z.: Mini 12, miniature mass spectrometer for clinical and other applications—introduction and characterization. Anal. Chem. ***86***, 2909–2916 (2014)
21. Luebkemann, F., Wanczek, K.P.: Miniature ICR cells. Int. J. Mass Spectrom. ***281***, 150–156 (2009)
22. Beauchamp, P., Hörst, S., Yelle, R., Cable, M., Neidholdt, E., Beauchamp, J., Hodyss, R., Briois, C., Thirkell, L., Willis, P., Nellis, G., Gianchandani, Y., Choukroun, M.: International Workshop on Instrumentation for Planetary Missions. Greenbelt. (2014)
23. Chen, E.X., Russell, Z.E., Amsden, J.J., Wolter, S.D., Danell, R.M., Parker, C.B., Stoner, B.R., Gehm, M.E., Glass, J.T., Brady, D.J.: Order

of Magnitude Signal Gain in Magnetic Sector Mass Spectrometry Via Aperture Coding. J. Am. Soc. Mass Spectrom. ***26***, 1633–1640 (2015)

24. Amsden, J.J., Herr, P.J., Landry, D.M.W., Kim, W., Vyas, R., Parker, C.B., Kirley, M.P., Keil, A.D., Gilchrist, K.H., Radauscher, E.J., Hall, S.D., Carlson, J.B., Baldasaro, N., Stokes, D., Di Dona, S.T., Russell, Z.E., Grego, S., Edwards, S.J., Sperline, R.P., Denton, M.B., Stoner, B.R., Gehm, M.E., Glass, J.T.: Proof of Concept Coded Aperture Miniature Mass Spectrometer Using a Cycloidal Sector Mass Analyzer, a Carbon Nanotube (CNT) Field Emission Electron Ionization Source, and an Array Detector. J. Am. Soc. Mass Spectrom. ***29***, 360–372 (2018)
25. Wright, S., Malcolm, A., Wright, C., O'Prey, S., Crichton, E., Dash, N., Moseley, R.W., Zaczek, W., Edwards, P., Fussell, R.J., Syms, R.R.: A microelectromechanical systems-enabled, miniature triple quadrupole mass spectrometer. Anal. Chem. ***87***, 3115–3122 (2015)
26. Welling, M., Schuessler, H.A., Thompson, R.I., Walther, H.: Ion/molecule reactions, mass spectrometry and optical spectroscopy in a linear ion trap. Int. J. Mass Spectrom. Ion Process. ***172***, 95–114 (1998)
27. Evans-Nguyen, T., Becker, L., Doroshenko, V., Cotter, R.J.: Development of a low power, high mass range mass spectrometer for Mars surface analysis. Int. J. Mass Spectrom. ***278***, 170–177 (2008)
28. Contreras, J.A., Murray, J.A., Tolley, S.E., Oliphant, J.L., Tolley, H.D., Lammert, S.A., Lee, E.D., Later, D.W., Lee, M.L.: Hand-portable gas chromatograph-toroidal ion trap mass spectrometer (GC-TMS) for detection of hazardous compounds. J. Am. Soc. Mass Spectrom. ***19***, 1425–1434 (2008)
29. Ouyang, Z., Wu, G., Song, Y., Li, H., Plass, W.R., Cooks, R.G.: Rectilinear ion trap: concepts, calculations, and analytical performance of a new mass analyzer. Anal. Chem. ***76***, 4595–4605 (2004)
30. Schwartz, J.C., Senko, M.W., Syka, J.E.: A two-dimensional quadrupole ion trap mass spectrometer. J. Am. Soc. Mass Spectrom. ***13***, 659–669 (2002)
31. Guan, S.: General phase modulation method for stored waveform inverse Fourier transform excitation for Fourier transform ion cyclotron resonance mass spectrometry. J. Chem. Phys. ***91***, 775–777 (1989)
32. Guan, S., Marshall, A.G.: Stored waveform inverse Fourier transform axial excitation/ejection for quadrupole ion trap mass spectrometry. Anal. Chem. ***65***, 1288–1294 (1993)
33. Guan, S., Marshall, A.G.: Stored waveform inverse Fourier transform (SWIFT) ion excitation in trapped-ion mass spectometry—theory and applications. Int. J. Mass Spectrom. Ion Process. ***157/158***, 5–37 (1996)
34. Snyder, D.T., Pulliam, C.J., Cooks, R.G.: Single analyzer precursor scans using an ion trap. Rapid Commun. Mass Spectrom. ***30***, 800–804 (2016)
35. Snyder, D.T., Pulliam, C.J., Cooks, R.G.: Linear mass scans in quadrupole ion traps using the inverse Mathieu q scan. Rapid Commun. Mass Spectrom. ***30***, 2369–2378 (2016)
36. Franzen, J.: The non-linear ion trap. Part 4. Mass selective instability scan with multipole superposition. Int. J. Mass Spectrom. Ion Process. ***125***, 165–170 (1993)
37. Franzen, J.: The non-linear ion trap. Part 5. Nature of non-linear resonances and resonant ion ejection. Int. J. Mass Spectrom. Ion Process. ***130***, 15–40 (1994)
38. Snyder, D.T., Pulliam, C.J., Wiley, J.S., Duncan, J., Cooks, R.G.: Experimental characterization of secular frequency scanning in ion trap mass spectrometers. J. Am. Soc. Mass Spectrom. ***27***, 1243–1255 (2016)
39. Guidugli, F., Traldi, P.: A phenomenological description of a black hole for collisionally induced decomposition products in ion-trap mass spectrometry. Rapid Commun. Mass Spectrom. ***5***, 343–348 (1991)
40. Morand, K.L., Lammert, S.A., Cooks, R.G.: Concerning 'Black Holes' in ion-trap mass spectrometry. Rapid Commun. Mass Spectrom. ***5***, 491 (2005)
41. Eades, D.M., Johnson, J.V., Yost, R.A.: Nonlinear resonance effects during ion storage in a quadrupole ion trap. J. Am. Soc. Mass Spectrom. ***4***, 917–929 (1993)
42. Splendore, M., Marquette, E., Oppenheimer, J., Huston, C., Wells, G.: A new ion ejection method employing an asymmetric trapping field to improve the mass scanning performance of an electrodynamic ion trap. Int. J. Mass Spectrom. ***191***, 129–143 (1999)
43. Snyder, D.T., Peng, W.-P., Cooks, R.G.: Resonance methods in quadrupole ion traps. Chem. Phys. Lett. ***668***, 69–89 (2017)
44. March, R.E.: Quadrupole ion traps. Mass Spectrom. Rev. ***28***, 961–989 (2009)
45. Li, X., Danell, R.M., Pinnick, V.T., Grubisic, A., van Amerom, F., Arevalo, R.D., Getty, S.A., Brinckerhoff, W.B., Southard, A.E., Gonnsen, Z.D., Adachi, T.: Mars Organic Molecule Analyzer (MOMA) laser desorption/ionization source design and performance characterization. Int. J. Mass Spectrom. ***422***, 177–187 (2017)
46. Snyder, D.T., Kaplan, D.A., Danell, R.M., van Amerom, F.H.W., Pinnick, V.T., Brinckerhoff, W.B., Mahaffy, P.R., Cooks, R.G.: Unique capabilities of AC frequency scanning and its implementation on a Mars Organic Molecule Analyzer linear ion trap. Analyst. ***142***, 2109–2117 (2017)
47. Balsiger, H., Altwegg, K., Bochsler, P., Eberhardt, P., Fischer, J., Graf, S., Jäckel, A., Kopp, E., Langer, U., Mildner, M., Müller, J., Riesen, T., Rubin, M., Scherer, S., Wurz, P., Wüthrich, S., Arijs, E., Delanoye, S., Keyser, J.D., Neefs, E., Nevejans, D., Rème, H., Aoustin, C., Mazelle, C., Médale, J.L., Sauvaud, J.A., Berthelier, J.J., Bertaux, J.L., Duvet, L., Illiano, J.M., Fuselier, S.A., Ghielmetti, A.G., Magoncelli, T., Shelley, E.G., Korth, A., Heerlein, K., Lauche, H., Livi, S., Loose, A., Mall, U., Wilken, B., Gliem, F., Fiethe, B., Gombosi, T.I., Block, B., Carignan, G.R., Fisk, L.A., Waite, J.H., Young, D.T., Wollnik, H.: Rosina – Rosetta orbiter spectrometer for ion and neutral analysis. Space Sci. Rev. ***128***, 745–801 (2007)
48. Rubin, M., Altwegg, K., Balsiger, H., Bar-Nun, A., Berthelier, J.J., Bieler, A., Bochsler, P., Briois, C., Calmonte, U., Combi, M., De Keyser, J., Dhooghe, F., Eberhardt, P., Fiethe, B., Fuselier, S.A., Gasc, S., Gombosi, T.I., Hansen, K.C., Hässig, M., Jäckel, A., Kopp, E., Korth, A., Le Roy, L., Mall, U., Marty, B., Mousis, O., Owen, T., Rème, H., Sémon, T., Tzou, C.Y., Waite, J.H., Wurz, P.: Molecular nitrogen in comet 67P/Churyumov-Gerasimenko indicates a low formation temperature. Science. ***348***, 232 (2015)
49. Mahaffy, P.R., Webster, C.R., Cabane, M., Conrad, P.G., Coll, P., Atreya, S.K., Arvey, R., Barciniak, M., Benna, M., Bleacher, L., Brinckerhoff, W.B., Eigenbrode, J.L., Carignan, D., Cascia, M., Chalmers, R.A., Dworkin, J.P., Errigo, T., Everson, P., Franz, H., Farley, R., Feng, S., Frazier, G., Freissinet, C., Glavin, D.P., Harpold, D.N., Hawk, D., Holmes, V., Johnson, C.S., Jones, A., Jordan, P., Kellogg, J., Lewis, J., Lyness, E., Malespin, C.A., Martin, D.K., Maurer, J., McAdam, A.C., McLennan, D., Nolan, T.J., Noriega, M., Pavlov, A.A., Prats, B., Raaen, E., Sheinman, O., Sheppard, D., Smith, J., Stern, J.C., Tan, F., Trainer, M., Ming, D.W., Morris, R.V., Jones, J., Gundersen, C., Steele, A., Wray, J., Botta, O., Leshin, L.A., Owen, T., Battel, S., Jakosky, B.M., Manning, H., Squyres, S., Navarro-González, R., McKay, C.P., Raulin, F., Sternberg, R., Buch, A., Sorensen, P., Kline-Schoder, R., Coscia, D., Szopa, C., Teinturier, S., Baffes, C., Feldman, J., Flesch, G., Forouhar, S., Garcia, R., Keymeulen, D., Woodward, S., Block, B.P., Arnett, K., Miller, R., Edmonson, C., Gorevan, S., Mumm, E.: The sample analysis at Mars investigation and instrument suite. Space Sci. Rev. ***170***, 401–478 (2012)
50. Brinckerhoff, W. B., Pinnick, V. T., Van Amerom, F. H., Danell, R. M., Arevalo, R. D., Atanassova, M. S., ... & Steininger, H. Mars Organic Molecule Analyzer (MOMA) mass spectrometer for ExoMars 2018 and beyond. In Aerospace Conference, 2013 I.E. (pp. 1–8). IEEE, Big Sky, MT (2013)